Published in Applied Physics Reviews, DOI: 10.1063/5.0224215, online on 05 Sep 2024, Vol. 11, No. 3, 031415.



# Ultrahigh Electromechanical Response in $(K,Na)NbO_3$-based Lead-Free Textured Piezoceramics

Yang Liu[1,2], Lang Bian[1], Rui Zhang[1,a], Jinhui Fan[1], Da Huo[1], Bingzhong Shen[1], Houbing Huang[3], Xiaoming Shi[4,a], Dawei Wang[1,a], Kui Yao[2,a]

[1] School of Instrumentation Science and Engineering, Harbin Institute of Technology, Harbin 150080, China

[2] Institute of Materials Research and Engineering (IMRE), A*STAR (Agency for Science, Technology and Research), Singapore 138634, Singapore

[3] School of Materials Science and Engineering and Advanced Research Institute of Multidisciplinary Science, Beijing Institute of Technology, Beijing 100081, China

[4] School of Mathematics and Physics, University of Science and Technology Beijing, Beijing 100083, China

[a)] Authors to whom correspondence should be addressed: ruizhang_ccmst@hit.edu.cn; 20220203@hit.edu.cn; shiming_870@163.com; k-yao@imre.a-star.edu.sg

**Abstract**

The progress of next-generation electromechanical devices is substantially reliant upon achieving high electromechanical coupling performance in piezoelectric materials. Here, a local stress regulation strategy is introduced to significantly enhance the overall electromechanical response of lead-free piezoceramics. A remarkable large piezoelectric coefficient ($d_{33}$) of ~800 pC $N^{-1}$ and longitudinal electromechanical coupling factor ($k_{33}$) of 88% are obtained in (K,Na)$NbO_3$ (KNN)-based textured piezoceramics. From both experimental examinations and theoretical simulation including phase-field analyses, it is found that the improved piezoelectric performance primarily stems from the stress-induced elastic field aligned with the preferred crystallographic orientation, which constrains the domain size, resulting in nanoscale short-range ordered domain structures. Such structures facilitate the flexible rotation of electric dipoles within coexisting phases due to flatten free energy distribution, thereby leading to the exceptionally large piezoelectric response. This understanding provides a valuable guidance for the design of novel lead-free piezoceramics with excellent piezoelectric performance.

**Key words:** KNN, textured ceramic, lead-free, piezoelectric performance

## 1. Introduction

Piezoelectric materials are garnering extensive attention in numerous applications such as sensors, transducers, and actuators, due to their inherent ability of the efficient conversion of electrical energy to mechanical energy and vice versa.[1] Lead-based piezoceramics, exemplified by $Pb(Zr,Ti)O_3$ (PZT), have been favored by researchers due to their superior performance with piezoelectric coefficient ($d_{33}$) ranging from 200 to 600 pC $N^{-1}$ and electromechanical coupling factor ($k_{33}$) from 0.50 to 0.75.[2] In the context of environmental conservation and regulatory constraints, lead-free piezoceramics like $BaTiO_3$ (BTO), $(Bi,Na)TiO_3$ (NBT), $BiFeO_3$ (BFO), and $(K,Na)NbO_3$ (KNN) are beginning to draw widespread research and industry interests.[3-10]

Various mechanisms and methods have been reported to enhance the piezoelectric properties of lead-based materials, such as morphotropic phase boundary (MPB), polar nanoregions (PNRs), polarization rotation, intermediate phases, domain engineering, and lattice distortions.[2, 4, 6, 9, 11-21] The relevant theories have been extensively applied from lead-based to lead-free materials, guiding the design of the lead-free materials with high piezoelectricity.[22, 23] The efforts on perovskite lead-free piezoceramics are elevated since Saito and colleagues achieved high piezoelectric performance ($d_{33}$: 432 pC $N^{-1}$, $k_p$: 0.61) in KNN-based ceramics using a texturing process.[24] Liu and Ren successfully established a tri-critical point of MPB in BTO-based ceramics, coexisting paraelectric cubic (C), ferroelectric rhombohedral (R) and tetragonal (T) phases.[4] Benefiting from the near disappearance of polarization anisotropy, BTO-based

ceramics exhibited a significantly enhanced $d_{33}$ of about 620 pC $N^{-1}$. In NBT-based ceramics, Tan et al. reported an electrostrain as high as 0.7%, originating from the phase transition between the relaxor ferroelectric phase (mixed R and T phases) and the R phase under an external electric field.[5] Utilizing compositional engineering method combined with a water-quenching process, Song et al. obtained BFO ceramics with a high $d_{33}$ above 400 pC $N^{-1}$ and a Curie temperature ($T_C$) above 400 °C.[3] Guided by phenomenological theory and phase-field simulations, Li et al. designed localized heterostructures in $Pb(Mg_{1/3}Nb_{2/3})O_3$-$PbTiO_3$ ceramics to modulate the free energy landscape. This innovative approach led to a $d_{33}$ of 1500 pC $N^{-1}$, even comparable to those of lead-based single crystals.[25] In ferroelectric materials, establishing the relationship between local structures and macroscopic properties is an effective strategy for optimizing their response characteristics.[26, 27] Utilizing advanced microstructural characterization techniques, Wang and colleagues discovered the presence of nanoscale local symmetries along the macroscopic average polarization direction.[28] This finding is instrumental in unraveling the origins of the large electrostrain observed in BFO-based ceramics at the local structure level. In $PbTiO_3$ materials, it is found macroscopic tensile pressure can suppress ferroelectricity because Pb-O and Ti-O hybridization weakens short-range repulsion, and compression enhances this effect.[29] However, the regulation of structures under local stress and the corresponding impact on the electromechanical performance of lead-free piezoelectric materials remain a not understood issue.

Based on the above considerations, in this work, a stress regulation strategy under

[001]-orientation is introduced in (K,Na)$NbO_3$ (KNN)-based textured piezoceramics, aiming to enhance the piezoelectric response. It was discovered that differential coefficients of thermal expansion between the template microcrystals and the matrix in the textured ceramics generate internal stresses during the sintering process. This stress can facilitate the switching of domains, effectively reducing the domain size and enhancing the piezoelectric response. Excitingly, compared to their randomly oriented counterparts, the textured ceramics demonstrated a significant improvement in overall electrical performance ($d_{33}$ ~800 pC $N^{-1}$, $k_p$ ~81.6%, $k_t$ ~56.9%, $k_{33}$ ~88.0% and $T_C$ ~235 °C). Both the experimental and theoretical modelling results supported our proposed underlying mechanisms for explaining the enhanced electromechanical response. This study provides significant guidance for the development of novel lead-free ceramics with high piezoelectric responses.

**2. Results and discussion**

Fig. 1(a) shows the X-ray diffraction (XRD) patterns of the $0.956K_{0.48}Na_{0.52}Nb_{0.96}Sb_{0.04}O_3$-$0.04Bi_{0.5}Na_{0.5}ZrO_3$-$0.004BaZrO_3$-$x$ vol. % $NaNbO_3$ (abbreviated as T-KNN-$x$NN) lead-free ceramics. All ceramics display a perovskite phase with no secondary phase detected. For T-KNN-$x$NN textured ceramics, diffraction peaks are predominantly {00l}, with nearly all other peaks disappearing, indicating a high degree of grain orientation along [001]. The {00l} peak intensity rapidly increases as the NN template content increases from 0.25 vol.% to 1 vol.%, with corresponding Lotgering factor ($F_{001}$) values rising from 93% to 97.1% in Fig. 1(b). The

high texture degree is attributed to the significant aspect ratio of NN templates and the high orientation under shear forces during tape casting.[30-32] The schematic representation of fabricating textured ceramics is shown in Fig. S1. The internal stress within the ceramics is adjusted by varying the template microcrystal content while maintaining a fixed chemical composition and high texture degree. The stress level in textured ceramics is expected to show significant differences compared to randomly oriented piezoceramics. As shown in Fig. 1(c), the linear fitting slopes for both randomly oriented (0 vol.%) and textured ceramics (0.5 vol.%) are negative, suggesting that both types of ceramics are in a compressive stress state, with residual stresses estimated at -39±9 and -155±43 MPa, respectively. Consequently, the residual stress level in T-KNN-0.5NN textured ceramic is nearly 2~6 times higher than that of randomly oriented ceramics (0 vol.%).

Temperature-dependent dielectric constant ($\varepsilon_r$) is shown in Fig. 1(d) and Fig. S2. T-KNN-*x*NN ceramics exhibit two dielectric anomaly peaks from -100 °C to 100 °C, corresponding to the R to orthorhombic (O, $T_{R\text{-}O}$) and O to T ($T_{O\text{-}T}$) phase transitions. Fig. 1(e) shows the temperature-dependent XRD patterns from 44.5° to 46.5° for randomly oriented ceramic and T-KNN-0.5NN textured ceramic. During heating, both ceramics undergo the following phase transitions: R-O phase $\xrightarrow{50\ ^\circ C}$ O-T phase $\xrightarrow{235\ ^\circ C}$ C phase. Temperature-dependent Raman spectroscopy measurements also provide strong evidence of phase evolution (Fig. S3), consistent with temperatures determined by variable-temperature XRD tests. Rietveld XRD full pattern fitting analysis indicates the presence of R phase (*R*3*m*，93.88%) and O phase (*Amm*2，6.12%) in the samples (Fig.

S4). Combining dielectric, XRD, and Raman data, the phase structure of all T-KNN-*x*NN samples is identified as coexisting R-O phase, indicating that T-KNN-*x*NN ceramics reside in the polymorphic phase boundary (PPB) near room temperature.

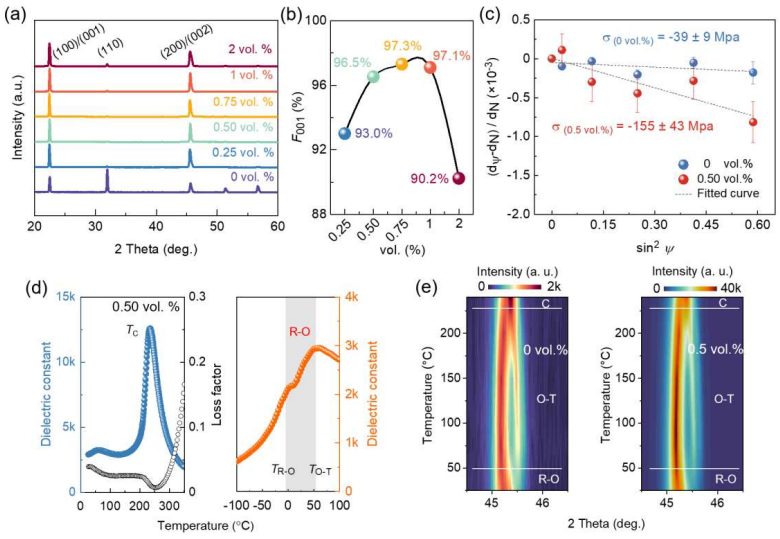


**FIG. 1.** Crystal structure and dielectric properties of KNN-based ceramics. (a) High-resolution XRD patterns of T-KNN-*x*NN ceramics. (b) Lotgering factor ($F_{001}$) as a function of NN template amount. (c) The d-spacing of (300) for randomly oriented ceramic and T-KNN-0.5NN textured ceramic at different tilt angle $\psi$ normalized to "no tilt" d-spacing, as a function of sin$^2$ $\psi$. (d) Temperature-dependent dielectric properties for T-KNN-0.5NN ceramic. (e) In-situ XRD patterns as a function of temperature for randomly oriented ceramic and T-KNN-0.5NN textured ceramic.

Fig. 2(a) shows the polarization-electric field (*P*-*E*) loops of T-KNN-*x*NN ceramics, exhibiting saturated hysteresis loops. It is clear that there is a significant enhancement in the $d_{33}$ for T-KNN-*x*NN ceramics upon the introduction of NN template microcrystals in Fig. 2(b), where the highest $d_{33}$ of 800±15 pC $N^{-1}$ is obtained for T-KNN-0.5NN ceramic. Furthermore, the phase angle of 81° for T-KNN-0.5NN ceramics indicates a high degree of polarization, as shown in Fig. 2(c).[8, 33] Remarkably, T-KNN-0.5NN ceramic exhibits exceptional electromechanical properties ($d_{33}$ of 800±15 pC $N^{-1}$, $k_p$~81.6%, $k_t$~56.9%, and $k_{33}$~88.0%). Fig. 2(d) compares the $d_{33}$ and $k_p$ values among various piezoceramics, including typical PZT-based and lead-free ceramics, underscoring the ultrahigh $d_{33}$ and $k_p$ values of the T-KNN-0.5NN ceramic developed in this study. To our knowledge, the comprehensive electromechanical performance of T-KNN-0.5NN ceramic represents the pinnacle in lead-free piezoceramics reported to date, significantly surpassing those of commercial PZT-5H ceramics. Combined with the low acoustic impedance of KNN-based textured ceramics, these advantages position T-KNN-0.5NN ceramic as competitive candidates for electromechanical devices, particularly in ultrasonic transducer applications where high electromechanical performance and low acoustic impedance contribute to expanded bandwidth and enhanced sensitivity.[34-37]

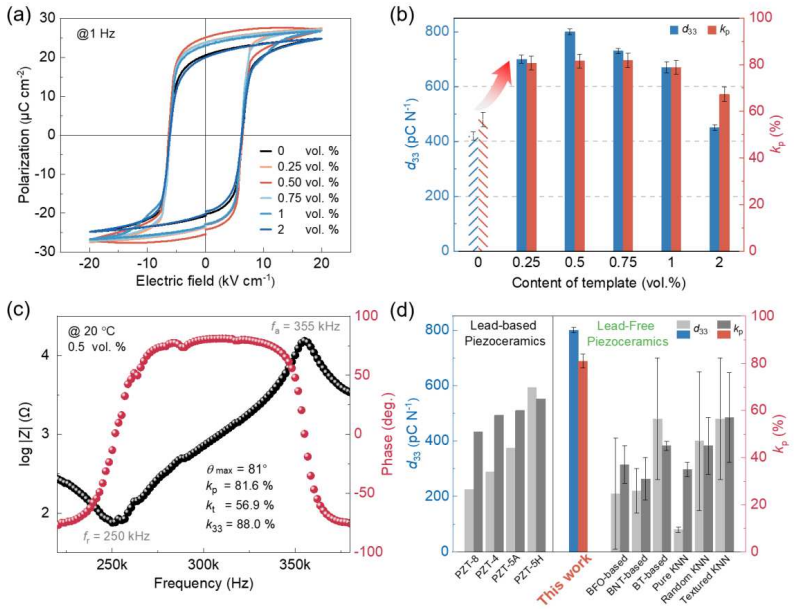


**FIG. 2.** Excellent electromechanical properties of T-KNN-0.5NN ceramic. (a) *P-E* loops of T-KNN-*x*NN ceramics. (b) $d_{33}$ and $k_p$ as a function of NN content. (c) Impedance and phase angle spectra for T-KNN-0.5NN ceramic. (d) Comparation of $d_{33}$ and $k_p$ in representative lead-based and lead-free piezoceramics.

Randomly oriented ceramics exhibit large-sized strip domain structures in Fig. 3(a), whereas T-KNN-0.5NN textured ceramic not only feature dense strip domains of approximately 5~40 nm but also display high-density domain configurations adjacent to long-range ordered domain structures in Fig. 3(b-c). Due to the lower energy of the nanoscale domain walls, these domains exhibit a more sensitive polarization response under external stimuli, leading to higher sensitivity to applied stress and electric field.[38-41] Local structures are precisely identified using scanning transmission electron

microscopy high-angle-annular-dark-field (STEM-HAADF). A polarization displacement map (Fig. 3d) is constructed based on Fig. S5. The polarization displacement primarily originates from B-site $Nb^{5+}$ and four adjacent A-site $K^+/Na^+$ ions. These displacements did not align in a uniform direction but were distributed in specific regions, forming areas of the same polarization direction within nano-domains approximately 2~4 nm in size. Fig. 3(e-f) show the c/a ratio of the unit cell and the B-site ion intensity map, respectively, revealing irregular and randomly distributed states, indicating strong fluctuation in the local elastic field.

Further exploration of the impact of stress on the ceramic microstructure is undertaken using Geometrical Phase Analysis (GPA) (Fig. 3g-h). The analysis reveals that the local strain $S_{xx}$ (~3%) along [001] in T-KNN-0.5NN textured ceramic is significantly higher than in randomly oriented ceramic (~1.3%), suggesting that the larger residual stress under preferred orientation may have resulted in the distribution of large strain within the ceramic. The STEM results clearly demonstrate that T-KNN-0.5NN ceramic is disturbed by the elastic field at the atomic scale, with short-range ordered domain configurations. The analysis shows that the crucial role of stress-induced elastic fields under the preferred orientation in suppressing domain size and forming nanoscale short-range ordered electric domain structures. The ensuing theoretical analysis reveal the existence of the elastic fields caused by the local residual stress can promote the flexible rotation of electric dipoles among the coexisting phases, ultimately enhancing the piezoelectric response.

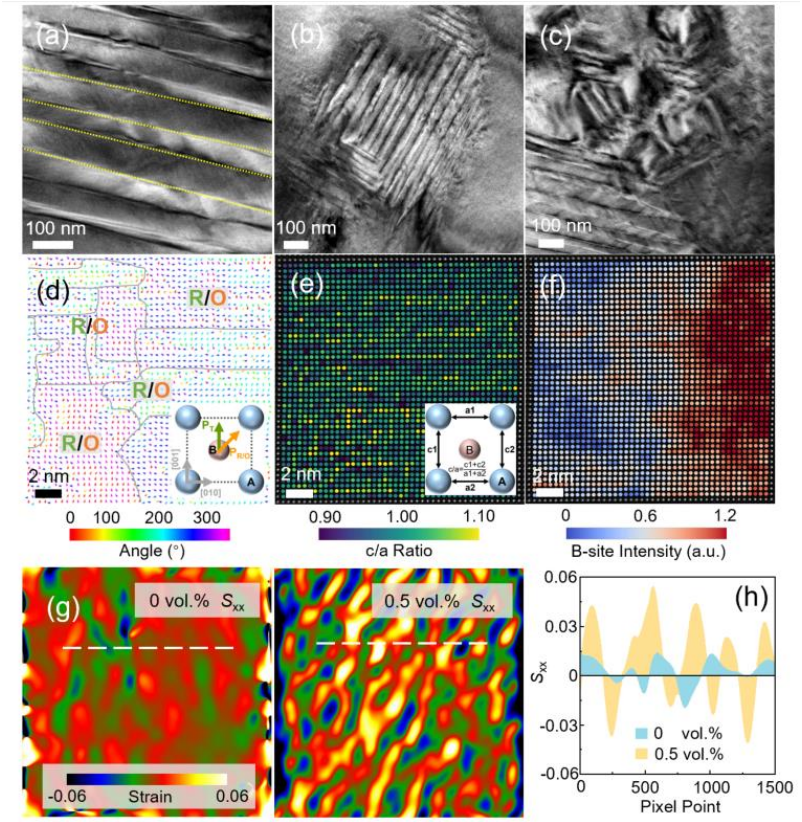


**FIG. 3.** Microstructure characterizations of T-KNN-*x*NN ceramics. (a) High-magnification bright-field TEM images of domain structures for randomly oriented ceramics. (b-c) TEM images of domain structures for T-KNN-0.5NN textured ceramic. (d) Atomic-resolution polarization vector image, where the inset diagram shows the schematic projection of the unit cell. (e) Unit cell c/a ratios for T-KNN-0.5NN textured ceramic. (f) Normalized intensities of the B-site sublattice for T-KNN-0.5NN textured ceramic. (g) Local strain field ($S_{xx}$) images calculated by GPA of randomly oriented ceramic and T-KNN-0.5NN textured ceramic. (h) Quantitative $S_{xx}$ analysis of the white dotted lines in g).

In Fig. 4(a) and Fig. S6, finite-element simulation is employed to analyze the local stress distribution of a single template model in sintered KNN textured ceramics. With the NN template microcrystals oriented along [001], the maximum local stress is observed to occur internally within the NN template microcrystals. With the decrease of the temperature after the sintering process, the stress between the template and matrix progressively intensified. This is a consequence of the mismatch in thermal expansion coefficients between the KNN-based powder and NN template microcrystals, generating significant local residual stress in the composite-like KNN-based textured ceramics during the formation of a solid solution and subsequent sintering cooling process. To investigate the piezoelectric effect, the relation of stress-domain structure-piezoelectric properties is established by phase-field simulation. As shown in Fig. 4(b-c), randomly oriented KNN ceramic samples have large domain sizes. When some template seeds are introduced into the matrix, irregular domain structures with significantly decreased domain sizes are formed. We calculated the magnitude of $d_{33}$ for both systems and observed a significant increase of nearly 35% in $d_{33}$ with introduction of the template seeds. This can be understood by the Landau free energy barriers profile in Fig. 4(d), in which the R and O phases in KNN system exhibit lower energy barriers compared to the T phase at room temperature. Based on Fig. 4(b-c), further calculations of the strain distribution corresponding to different domain structures (Fig. 4e-f, Fig. S7) revealed that the overall strain in textured ceramics is significantly higher than in randomly oriented ceramics, especially at the position of the template. Due to the existence of local stress concentration and fluctuations at the

interface between the template and the matrix phase, the phase structure fluctuations occur in the regions nearby, inducing the formation of fragmented domain structures. The study indicates that appropriately controlling the elastic field induced by stress can suppress domain size and facilitate the rotation of electric dipoles among coexisting phases, thereby significantly enhancing the piezoelectric response. The phase-field simulation results are well aligned with our experimental observations, revealing the microstructures characterized with coexisting phases in the textured ceramics. This theoretically explains the underlying mechanism for enhancing the piezoelectric properties of textured ceramics with residual local stress regulated by the preferred crystallographic orientation.

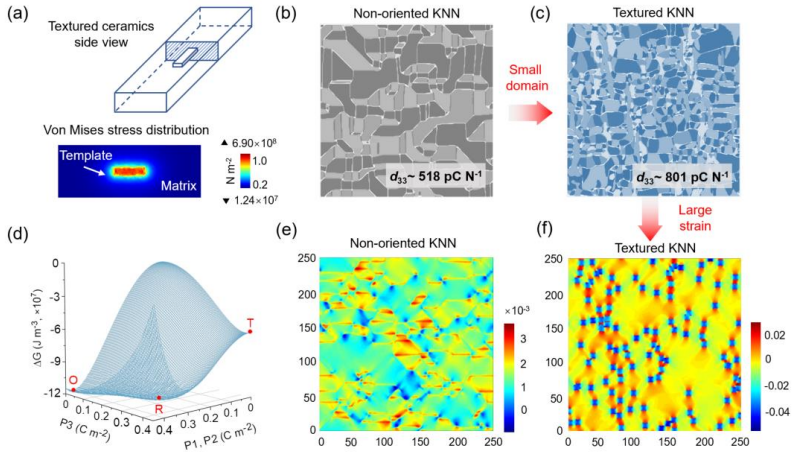


**FIG. 4.** Finite-element and phase-field simulations of T-KNN-*x*NN ceramics. (a) Schematics of KNN-based lead-free textured ceramics and local distribution of Von Mises stresses based on finite-element simulations. (b-c) Phase-field simulations of the domain structures for randomly oriented

KNN and textured KNN ceramics. (d) Landau free energy barrier of the KNN systems along the polarization rotation path. (e-f) Phase-field simulations of the strain distribution (z direction) for randomly oriented KNN and textured KNN ceramics.

## 3. Conclusions

In this work, leveraging a stress regulation strategy, KNN-based textured lead-free piezoceramics with [001]-orientation have exhibited outstanding comprehensive electromechanical performance ($d_{33}$ ~800 pC $N^{-1}$, $k_p$ ~81.6%, $k_t$ ~56.9%, $k_{33}$ ~88.0% and $T_C$ ~235 °C). This technical breakthrough stems from the introduction of local residual stress in the obtained textured ceramics, in contrast to randomly oriented counterparts. Both experimental observations and theoretical simulations, reveal that manipulated stress-induced elastic fields can suppress the size of electric polarization zones, leading to the formation of nanoscale, short-range ordered domain structures. This facilitates the flexible rotation of electric dipoles among the coexisting phases, thereby significantly enhancing the piezoelectric response. Our theoretical understanding provides a valuable guideline for designing piezoelectric materials with enhanced properties.

## Supplementary Material

See supplementary material for detailed experimental and characterizations on structure and property of textured ceramics (Figs. S1-S17, Tables S1-S2).

## Acknowledgements

Y. Liu and L. Bian contributed equally to this work. This research was financially

supported by the National Natural Science Foundation of China (Grant No. 11974093), Heilongjiang Touyan Innovation Team Program (Grant No. XNAUEA5640201720-09), Medical Engineering (Science) cross research fund of Harbin Institute of Technology (Grant No. IR2021238). The author from IMRE acknowledges partial supports from A*STAR, under RIE2020 AME Programmatic Fund (Grant No. A20G9b0135), Singapore.

**References**

[1] T.R. Shrout, S.J. Zhang. J. Electroceram. **19**, 113-126 (2007).

[2]E.W. Sun, W.W. Cao. Prog. Mater. Sci. **65**, 124-210 (2014).

[3]M.H. Lee, D.J. Kim, J.S. Park, S.W. Kim, T.K. Song, M.H. Kim, W.J. Kim, D. Do, I.K. Jeong. Adv. Mater. **27**, 6976-6982 (2015).

[4]W.F. Liu, X.B. Ren. Phys. Rev. Lett. **103**, 257602 (2009).

[5]X.M. Liu, X.L. Tan. Adv. Mater. **28**, 574-578 (2016).

[6]H. Tao, H.J. Wu, Y. Liu, Y. Zhang, J.G. Wu, F. Li, X. Lyu, C.L. Zhao, D.Q. Xiao, J.G. Zhu, S.J. Pennycook. J. Am. Chem. Soc. **141**, 13987-13994 (2019).

[7]D.W. Wang, Z.M. Fan, G.H. Rao, G. Wang, Y. Liu, C.L. Yuan, T. Ma, D.J. Li, X.L. Tan, Z.L. Lu, A. Feteira, S.Y. Liu, C.G. Zhou, S.J. Zhang. Nano Energy **76**, 104944 (2020).

[8]Y.X. Liu, W.B. Qu, H.C. Thong, Y. Zhang, Y.F. Zhang, F.Z. Yao, T.N. Nguyen, J.W. Li, M.H. Zhang, J.F. Li, B. Han, W. Gong, H.J. Wu, C.F. Wu, B. Xu, K. Wang. Adv. Mater. **34**, 2202558 (2022).

[9]P. Li, J.W. Zhai, B. Shen, S.J. Zhang, X.L. Li, F.Y. Zhu, X.M. Zhang. Adv. Mater. **30**,

1705171 (2018).

[10]B.K. Kim, K.S. Park, S.H. Key, Y.S. Cho, Adv. Energy Mater. **13**, 37 (2023).

[11]F. Li, S.J. Zhang, Z. Xu, L.Q. Chen. Adv. Funct. Mater. **27**, 1700310 (2017).

[12]L.Y. Yang, H.B. Huang, Z.Z. Xi, L.M. Zheng, S.Q. Xu, G. Tian, Y.Z. Zhai, F.F. Guo, L.P. Kong, Y.G. Wang, W.M. Lü, L. Yuan, M.L. Zhao, H.W. Zheng, G. Liu. Nat. Commun. **13**, 2444 (2022).

[13]F. Li, L. Jin, Z. Xu, S.J. Zhang, Appl. Phys. Rev. **1**, 011103 (2014)

[14]A. Kumar, N.B. Jonathon, C.B. Preston, J.C. Matthew, S.J. Zhang, C.D. Elizabeth, L.I. Douglas, M.L.B. James. Nat. Mater. **20**, 62-67 (2021).

[15]M. Eremenko, V. Krayzman, A. Bosak, H.Y. Playford, K.W. Chapman, J.C. Woicik, B. Ravel, I. Levin. Nat. Commun. **10**, 2728 (2019).

[16]B. Noheda, D.E. Cox, G. Shirane, S.E. Park, L.E. Cross, Z. Zhong. Phys. Rev. Lett. **86**, 3891-3894 (2001).

[17]J.G. Wu, D.Q. Xiao, J.G. Zhu. Chem. Rev. **115**, 2559-2595 (2015).

[18]Q. Liu, Y. Zhang, J. Gao, Z. Zhou, H. Wang, K. Wang, X. Zhang, L. Li, J.-F. Li. Energy Environ. Sci. **11**, 3531-3539 (2018).

[19]T. Zheng, H. Wu, Y. Yuan, X. Lv, Q. Li, T. Men, C. Zhao, D. Xiao, J. Wu, K. Wang, J.F. Li, Y. Gu, J. Zhu, S.J. Pennycook, Energy Environ. Sci. **10**, 528-537 (2017).

[20]J. Lin, G. Ge, J. Li, J. Qian, K. Zhu, Y. Wei, C. Shi, G. Li, F. Yan, W. Li, J. Zhang, J. Zhai, H. Wu, Adv. Funct. Mater. **33**, 2303965 (2023).

[21]G. Liu, L.P. Kong, Q.Y. Hu, S.J. Zhang, Appl. Phys. Rev. **7**, 021405 (2020).

[22]H.J. Liu, H.J. Wu, K.P. Ong, T.N. Yang, P. Yang, P.K. Das, X. Chi, Y. Zhang, C.Z.

Diao, W.K.A. Wong, E.P. Chew, Y.F. Chen, C.K.I. Tan, A. Rusydi, M.B.H. Breese, D. J. Singh, L.Q. Chen, S.J. Pennycook, K. Yao, Science. **369**, 292-297 (2020).

[23]M. Waqar, H.J. Wu, K.P. Ong, H.J. Liu, C.J. Li, P. Yang, W.J. Zang, W.H. Liew, C.Z. Diao, S.B. Xi, D.J. Singh, Q. He, K. Yao, S.J. Pennycook, J. Wang, Nat. Commun. **13**, 3922 (2022).

[24]Y. Saito, H. Takao, T. Tani, T. Nonoyama, K. Takatori, T. Homma, T. Nagaya, M. Nakamura. Nature. **432**, 84-87 (2004).

[25]F. Li, D.B. Lin, Z.B. Chen, Z.X. Cheng, J.L. Wang, C.C. Li, Z. Xu, Q.W. Huang, X.Z. Liao, L.Q. Chen, T.R. Shrout, S.J. Zhang. Nat. Mater. **17**, 349-354 (2018).

[26]H. Wu, S.C. Ning, M. Waqar, H.J. Liu, Y. Zhang, H.H. Wu, N. Li, Y. Wu, K. Yao, T. Lookman, X.D. Ding, J. Sun, J. Wang, S.J. Pennycook. Nat. Commun. **12**, 2841 (2021).

[27]M. Waqar, J.W. Chai, L.M. Wong, P.C. Lim, S.T. Chen, W.H. Liew, S.J. Wang, J.S. Chen, Q. He, K. Yao, J. Wang, Nano Lett. **23**, 11026-11033 (2023).

[28]G. Wang, T.F. Hu, W.X. Zhu, Z.L. Lu, A. Kleppe, M.D. Lopez, A. Feteira, D.C. Sinclair, Z.Q. Fu, H.B. Huang, D.W. Wang, I.M. Reaney. Phys. Rev. Lett. **130**, 076801 (2023).

[29]R.E. Cohen, Nature. **358**, 136-138 (1992).

[30]G.L. Messing, S. Trolier-McKinstry, E.M. Sabolsky, C. Duran, S. Kwon, B. Brahmaroutu, P. Park, H. Yilmaz, P.W. Rehrig, K.B. Eitel, E. Suvaci, M. Seabaugh, K.S. Oh. Crit. Rev. Solid. State. **29**, 45-96 (2004).

[31]L. Bian, X.D. Qi, K. Li, Y. Yu, L.J. Liu, Y.F. Chang, W.W. Cao, S.X. Dong. Adv. Funct. Mater. **30**, 202001846 (2020).

[32]Y.K. Yan, L.D. Geng, L.F. Zhu, H.Y. Leng, X.T. Li, H.R. Liu, D.B. Lin, K. Wang, Y.U. Wang, P. Shashank. Adv. Sci. **9**, 2105715 (2022).

[33]Y. Liu, J. Fan, X. Qi, B. Shen, R. Zhang, K. Yao, Nano Energy, **128**, 109972 (2024).

[34]S.J. Zhang, F. Li, X.N. Jiang, J.W. Kim, J. Luo, X.C. Geng. Prog. Mater. Sci. **68**, 1-66 (2015).

[35]Q.F. Zhou, K.H. Lam, H.R. Zheng, W.B. Qiu, K.K. Shung. Prog. Mater. Sci. **66**, 87-111 (2014).

[36]Y. Liu, B.Z. Shen, L. Bian, J.G. Hao, B. Yang, R. Zhang, W.W. Cao. ACS Appl. Mater. Interfaces. **15**, 47221-47228 (2023).

[37]Y. Liu, K. Zhu, B.Z. Shen, J.P. Ma, L. Bian, R. Zhang, W.W. Cao. Ceram. Int. **49**, 40450-40456 (2023).

[38]X. Lv, X.X. Zhang, J.G. Wu. J. Mater. Chem. A. **8**, 10026-10073 (2020).

[39]K.A. Schönau, M. Knapp, H. Fuess, R.A. Eichel, H. Kungl, J.M. Hoffmann. Phys. Rev. B. **75**, 184117 (2007).

[40]R. Theissmann, L.A. Schmitt, J. Kling, R. Schierholz, K.A. Schönau. J. Appl. Phys. **102**, 024111 (2007).

[41]K. Wang, F.Z. Yao, W. Jo, D. Gobeljic, V.V. Shvartsman, D.C. Lupascu, J.F. Li, J. Rödel. Adv. Funct. Mater. **23**, 4079-4086 (2013).